

FLOW PATTERN CONTROL IN MICROCHANNELS BY MEANS OF WALL SURFACE PATTERNING

K. Fushinobu, M. Nakata, M. Tokushige and K. Okazaki

Tokyo Institute of Technology, Meguro-ku Tokyo, JAPAN; fushinok@mech.titech.ac.jp

ABSTRACT

Flow pattern control in EOF-driven microchannels has been investigated. Part of the SiO₂ channel wall has been replaced with other oxide to create flow pattern change. Experiment has shown the feasibility of flow control concept. Numerical calculation has been performed in order to examine the parameters.

INTRODUCTION

Recent progress of the surface micromachining technology expands the frontier of engineering applications. Some of them include microsystems that handle tiny amount of liquid for various applications. The microsystems, such as μ TAS or microreactors, conduct reagents preparation, chemical reaction and their analysis automatically within a single microchip. One of the advantage of these microsystems is that it can save the time for the process due to the small system size with small amount of chemicals.

In many cases of chemical reaction, the rate limiting factor can be a diffusion process. The above microsystems have a same kind of technological challenge. Since the chemical reaction of reagents requires mixing process, typical μ TAS or microreactor has a microchannel where two or more chemicals are introduced and mixed together, followed by their chemical reaction. Since the microchannel has a width of typically less than hundreds of μ m, the Reynolds number is typically on the order of 0.1 to 10. The flow in the microchannel is laminar, and the mixing of the chemicals is a diffusion process. Since the turbulent mixing is not expected, the mixing may be a time consuming process. Microchannels with typically 100 μ m or wider, for instance, require long time period for complete mixing, and the time has to be reduced by developing a novel microfluidic mixing device.

There have been a several types of microfluidic mixing devices proposed so far [1-6]. Each one of them has an advantage as a mixing device, and the following issues has to be considered for improving the devices: Small moving parts in general decreases the system reliability due to the process failure and the device failure under operation

conditions. Complicated structure increases the fabrication process complexity and leads to process failure or cost issue. Simplicity of the whole system including peripheral equipment as well as the device itself is another important figure of merit.

Recently, the authors have proposed a novel mixing concept for microfluidic devices and exhibited its feasibility for EOF (electroosmotic flow)-pumped microchannels [7, 8]. In our previous study [8], an SiO₂ microchannel is fabricated, and part of the channel wall is covered with a patterned Al₂O₃ thin film. Due to the difference of the surface zeta potential, the surface charge is different on the Al₂O₃ thin film that creates local EOF velocity difference. This phenomenon is clearly observed in experiment where flow pattern is drastically changed with and without the Al₂O₃ thin film. Numerical calculation proposed possible mixing enhancement effect.

In this study, we examine a numerical study of the mixing enhancement effect in EOF-pumped microchannel. The patterning geometry and the material are changed to see the mixing enhancement effect.

PRINCIPLE OF EOF MIXING

Electroosmotic flow (EOF)

When a glass capillary is filled with electrolyte solution and is applied with a high voltage, the solution flows along the capillary channel. This phenomenon is called electroosmotic flow (EOF.) The physics behind the phenomenon is explained in the following manner and schematically shown in Fig. 1(a): when a metal oxide

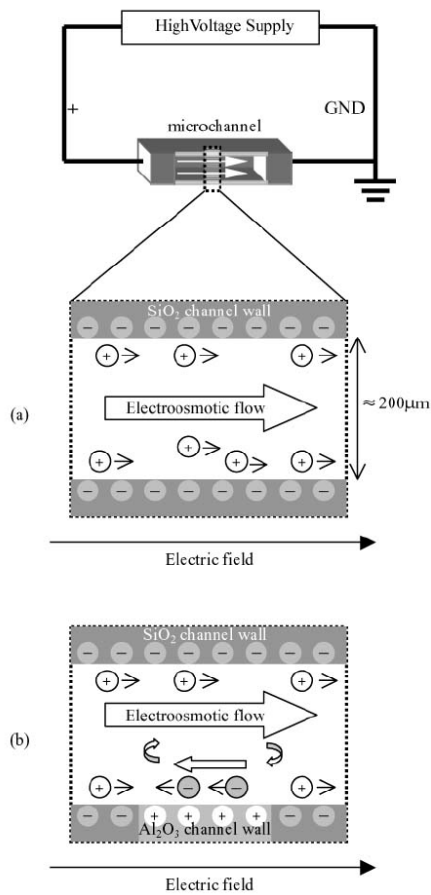


Fig.1 A schematic of regular and proposed microchannels driven with EOF
 (a) Regular microchannel for fluid pumping
 (b) Proposed fluid pumping microchannel with mixing enhancement

surface is exposed to electrolyte solution, the solid surface is charged either positively or negatively depending on the combination of the solid surface property and liquid pH [9]. Counter-ions then appear in the electrolyte in the vicinity of the contact surface. When the high voltage is applied, the ions move toward the direction of electric field accompanied by the bulk fluid flow. The velocity of the bulk liquid flow is called EOF velocity and is represented by Eq. (1) (Smoluchowski's equation) [10]

$$u = -\frac{\epsilon_r \epsilon_0}{\mu} \zeta E \quad (1)$$

where ζ is the electrical potential at the slip plane in the electric double layer and called zeta potential. The value of the zeta potential is determined depending on the relation between the channel wall material and the pH of the electrolyte. The zeta potential value becomes zero at certain liquid pH, and this pH value is called isoelectric point, pH_0 . The isoelectric point is therefore a unique property for each metal oxide; for instance, the value of pH_0 is equal to 2 for SiO_2 , 9 for Al_2O_3 and 10 for NiO [11, 12]. When pH_0 is lower than the electrolyte's pH, the oxide surface charges negatively, while the pH_0 is higher, the surface charges

positively. Different value of pH_0 , which means different channel wall material, therefore leads to different EOF velocity.

Recent progress of the surface micromachining technology expands the frontier of engineering applications. Some of them include microsystems that handle tiny amount of liquid for various applications. The microsystems, such as μ TAS or microreactors, conduct reagents preparation, chemical reaction and their analysis automatically within a single microchip. One of the advantages of these microsystems is that it can save the time for the process due to the small system size with small amount of chemicals.

Liquid mixing by using ζ -potential patterning; a novel technique

Since the flow velocity of liquid in a microchannel can be varied by changing the wall material of the channel, one can replace part of a wall material with a different metal oxide in order to change the flow field locally. This flow pattern change may result in expanding the interface area of liquids to be mixed and lead to an enhancement of liquid mixing. Figure 1(b) shows a schematic of the mixing device concept. It is basically an EOF fluid pumping microchannel. The only difference with Fig. 1(a) is that part of the channel wall is replaced with a different metal oxide material. Since the EOF velocity is changed locally, the flow pattern is also expected to be changed.

This mixing device has various advantages over the conventional microfluidic mixing devices. It is easy to fabricate; fabrication of the device requires only one more lithography process to be added to the conventional microchannel fabrication process. Also, the structure is simple; both reliability and cost advantages can be pointed out due to its simplicity. It does not require small moving parts, which degrade the device reliability.

EXPERIMENT

Prior to the numerical results and discussions, our previously reported experimental results are briefly described in order to help understanding the computation section.

Sample fabrication

Two types of microchannels are fabricated. One is a regular microchannel in which entire channel wall is made of a single material, and we call this a microchannel of *Type I* in this paper. This type is fabricated in order to measure the EOF velocity in a microchannel; it is made of either SiO_2 or Al_2O_3 . And the other type is made in order to demonstrate the flow pattern change, which is made of mainly SiO_2 and is partly Al_2O_3 sputtered. We call this a microchannel of *Type II*. The difference of two types is basically the local patterning of Al_2O_3 thin film.

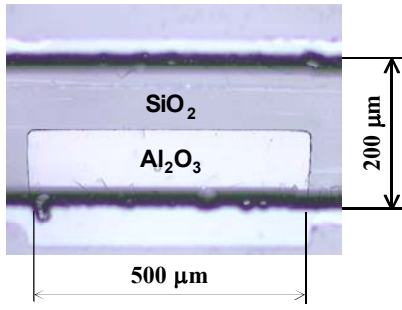


Fig.2 Top view of the fabricated microchannel Type II

In the first type of the microchannels, the wall material is either SiO₂ or Al₂O₃. Both were fabricated on a Pyrex (#7059) glass chip with a size of 20mm × 14mm × 0.5mm. They were fabricated by buffered HF etching. For Al₂O₃ microchannel, the etched channel was covered by film deposition technique. The length of the microchannel is 15mm, and the width is about 300μm. Details of the fabrication process is described in our previous report [8]. In the fabrication of second type microchannel, following lift-off process is added to deposit Al₂O₃ thin film pattern on the bottom surface of the first type microchannel. Figure 2 shows a microscope image of a fabricated sample for flow pattern visualization experiment. Both types of the microchannels were completed by encapsulating the ditch on a Pyrex substrate with polydimethylsiloxane (PDMS) film.

Measurement

Before the imaging of flow pattern change, the EOF velocities in SiO₂ and Al₂O₃ microchannels were measured by using the type I microchannel, respectively [8]. The measured velocity for SiO₂ is compared with previous data [13] and gives good agreement. Also, the flow direction of the fluid under same electric field is confirmed to be opposite for Al₂O₃ microchannel due to the relationship between the isoelectric points for SiO₂ (≈ 2) and Al₂O₃ (≈ 9.) and the electrolyte pH (= 5.8.) The EOF mobility, $\mu_{EOF} = u/E$, is obtained to be 2.35×10^{-8} m²/(V·s) for SiO₂ and -3.00×10^{-8} m²/(V·s) for Al₂O₃. The zeta potential is then obtained from Eq. (1) by using these values and given as $\zeta_{SiO_2} = -29$ mV for SiO₂ and $\zeta_{Al_2O_3} = 37$ mV for Al₂O₃.

Fabricated SiO₂ and Al₂O₃ microchannels are confirmed to have opposite flow directions for electrolyte with pH = 5.8. Next, we conducted an experiment to exhibit the proposed flow pattern change in an SiO₂ microchannel with Al₂O₃ thin film patterned on the channel bottom, shown in Fig. 2. The flow pattern in the microchannel is visualized by using a microscope CCD, and the images are recorded in PC. Polystyrene particles of average diameter $d = 2 \mu\text{m}$ are used as tracers for visualizing the flow pattern. Figure 3 shows a top view of the tracer particle trajectories in the microchannel. As we discussed above, the EOF velocity on SiO₂ and Al₂O₃ surfaces have different values, and therefore the particles should exhibit flow pattern

change. The figure clearly shows this trend and exhibits the feasibility of using this type of microchannel for mixing enhancement.

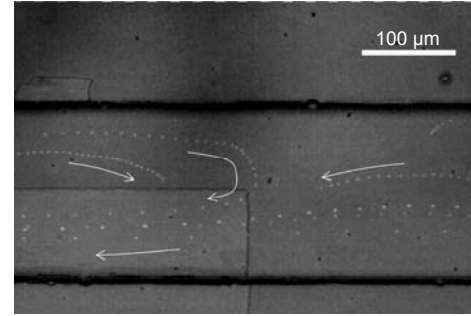


Fig.3 Top view of the microchannel Type II; tracer trajectories

NUMERICAL CALCULATION

Modeling

The microchannel of Type II (Fig. 2) is confirmed to exhibit flow pattern change experimentally. In order to examine the mixing enhancement effect quantitatively, numerical calculation is carried out. Figure 4 shows a schematic of the computational domain. Two dimensional domain of 1mm length and 200 μm width is solved. In the calculation, three types of channels are examined. The first one has SiO₂ walls. The others have Al₂O₃ patterning on one side or both sides of the channel walls. These patterns are examined in order to see whether the Al₂O₃ patterning is effective for mixing enhancement or not.

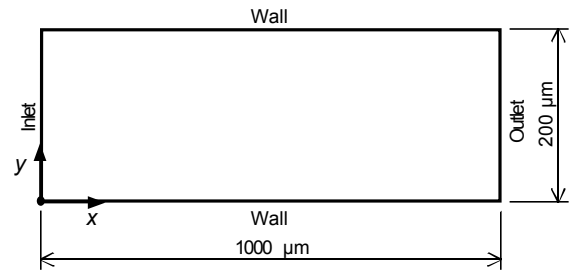


Fig.4 Dimensions and the coordinate of the computational domain; top view of a microchannel where part of the side walls (denoted as "Wall" in the figure) are patterned to have different zeta potential value.

We use the flow field and the electrical potential analysis presented by Yang et al. [14] and combine the concentration field calculation. The governing and constitutive equations are as follows.

$$\frac{\partial^2 \psi}{\partial x^2} + \frac{\partial^2 \psi}{\partial y^2} = \frac{2ze n_0}{\epsilon_r \epsilon_0} \sinh \frac{ze\psi}{k_b T} \quad (2)$$

$$\rho_e = -2ze n_0 \sinh \frac{ze\psi}{k_b T} \quad (3)$$

$$\frac{\partial u}{\partial x} + \frac{\partial v}{\partial y} = 0 \quad (4)$$

$$\rho_m u \frac{\partial u}{\partial x} + \rho_m v \frac{\partial u}{\partial y} = -\rho_m \frac{\partial P}{\partial x} + \mu \left(\frac{\partial^2 u}{\partial x^2} + \frac{\partial^2 u}{\partial y^2} \right) + \rho_e E \quad (5)$$

$$\rho_m u \frac{\partial v}{\partial x} + \rho_m v \frac{\partial v}{\partial y} = -\rho_m \frac{\partial P}{\partial y} + \mu \left(\frac{\partial^2 v}{\partial x^2} + \frac{\partial^2 v}{\partial y^2} \right) \quad (6)$$

$$u \frac{\partial c}{\partial x} + v \frac{\partial c}{\partial y} = D \left(\frac{\partial^2 c}{\partial x^2} + \frac{\partial^2 c}{\partial y^2} \right) \quad (7)$$

where ε_r ($= 78.5$), ρ_m ($= 996.7 \text{ kg/m}^3$) and μ ($= 854.4 \text{ } \mu\text{Pa}\cdot\text{s}$) are the dielectric constant, density, and the viscosity of the electrolyte solution, e is the unit electrical charge, n_0 ($= 3.0 \times 10^{25} \text{ m}^{-3}$, 50 mM) is the KCl ion concentration, ε_0 is the permittivity in vacuum, k_b is the Boltzmann constant and D ($= 1.0 \times 10^{-10} \text{ m}^2/\text{s}$) is the diffusion coefficient. The value of D is chosen as a typical value for reagents considered in applications. Temperature, T , is considered to be constant at 300 K. The boundary conditions are given as

$$\begin{aligned} & \text{(inlet)} \\ & \frac{\partial \psi}{\partial x} = 0, \quad \frac{\partial u}{\partial x} = 0, \quad \frac{\partial v}{\partial x} = 0, \quad \frac{\partial P}{\partial x} = 0, \\ & c = \begin{cases} 0 & (0 \leq y \leq W/2) \\ c_0 & (W/2 < y \leq W) \end{cases} \end{aligned} \quad (8)$$

$$\begin{aligned} & \text{(outlet)} \\ & \frac{\partial \psi}{\partial x} = 0, \quad \frac{\partial u}{\partial x} = 0, \quad \frac{\partial v}{\partial x} = 0, \quad \frac{\partial P}{\partial x} = 0, \quad \frac{\partial c}{\partial x} = 0 \end{aligned} \quad (9)$$

$$\begin{aligned} & \text{(wall)} \\ & \psi = \begin{cases} \zeta_{SiO_2} & (\text{SiO}_2 \text{ wall}) \\ \zeta_{Al_2O_3} & (\text{Al}_2\text{O}_3 \text{ wall}) \end{cases}, \\ & u = 0, \quad v = 0, \\ & \frac{\partial P}{\partial y} = 0, \quad \frac{\partial c}{\partial y} = 0 \end{aligned} \quad (10)$$

The electrical potential, ψ , is obtained by solving the Poisson-Boltzmann equation (Eq. (2)), and the charge density, ρ_e , is calculated by using Eq. (3). The flow field is obtained by solving Eqs. (4)-(6) with SIMPLER algorithm [15]. The concentration, c , is then calculated by solving Eq. (7).

Other parameters used in the calculation are as follows; initial concentration of reagent $c_0 = 1.0 \times 10^{-2} \text{ mol/l}$ and the electric field $E = 10^4 \text{ V/m}$.

Results and discussions

Effect of the pattern length, L_p , is discussed where the Al_2O_3 is attached at the bottom wall as shown in Fig. 5.

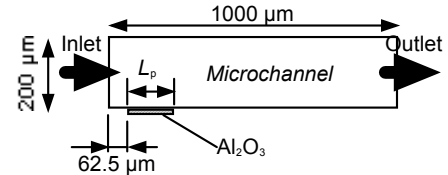


Fig.5 Configuration of the Al_2O_3 patterning for Figs. 6, 7 and 8. Effect of pattern length, L_p , is discussed.

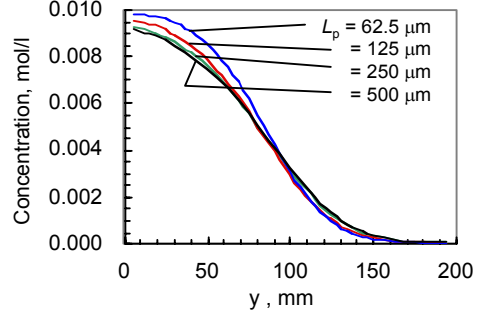


Fig.6 Calculated concentration profile at the channel outlet. The channel configuration is shown in Fig. 5

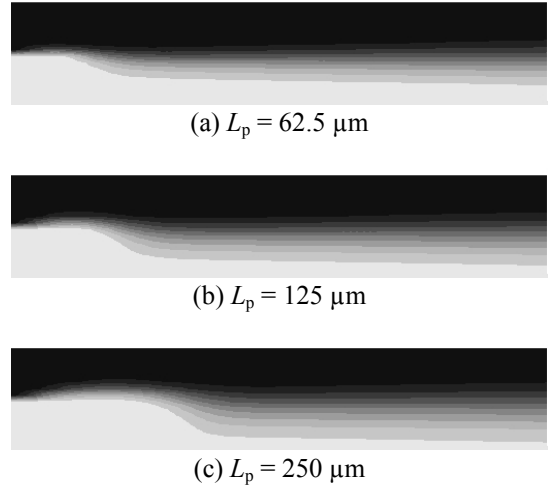


Fig.7 Calculated concentration distribution in a microchannel. The channel configuration is shown in Fig.5

Figure 6 shows the effect of the patterned Al_2O_3 size; the sizes are 62.5, 125, 250 and 500 μm , respectively. The figure shows the concentration profile of reagent at the channel outlet. Without mixing, the profile is a step function; $c = 1.0 \times 10^{-2}$ below $y \leq 100 \text{ } \mu\text{m}$, and $c = 0$ below $y \geq 100 \text{ } \mu\text{m}$. As the mixing proceeds, the profile gradient decreases, and the concentration profile finally reaches a flat line where $c = 0.5 \times 10^{-2}$. As the size increases, the concentration profiles show clear difference; the mixing effect at the channel outlet increases with increasing size of Al_2O_3 and saturates at longer cases. This trend can be also seen in Fig. 7, where the two-dimensional concentration distribution in the channel is exhibited. The darker (black) area represents higher concentration of reagent, and the lighter (white) area does lower value. The figure shows that the mixing enhancement clearly appears at the downstream

side of the Al_2O_3 pattern; as shown in Fig. 7 (a), the concentration distribution shows drastic change where the concentration contour is curved (mixing area), then the streamline recovers the straight pattern that should appear in a channel without Al_2O_3 pattern.

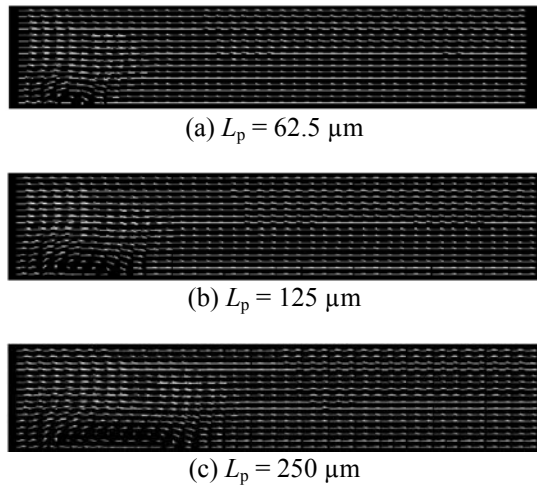


Fig.8 Calculated velocity vector distribution in a microchannel. The channel configuration is shown in Fig.5

Figure 8 shows the velocity vector in the channel. A recirculation region is created on the Al_2O_3 pattern due to its opposite EOF velocity to the SiO_2 channel, and the flow bending is clearly observed. Also, the lateral (y-direction) size of the recirculation region becomes larger for longer Al_2O_3 case and saturates at the longest case. The mixing enhancement effect mainly appears at the region where the flow field is curved to have lateral component to the bulk channel flow direction, and it is clearly observed that the longer the Al_2O_3 pattern is, the larger the mixing enhancement effect is. These results suggest that pattern length of $250\ \mu\text{m}$ is long enough for maximizing the mixing effect for this specific channel geometry and wall materials. Note that in these cases, a straight flow field in the bulk flow direction is recovered at the channel outlet.

For Al_2O_3 pattern with $250\ \mu\text{m}$ length case, effect of the patterning position from the inlet, L_u , is examined as shown in Fig. 9. Figure 10 shows the concentration profile at the channel outlet. Considering the concentration gradient, dc/dy , at $c = 0.5 \times 10^{-2}$, the figure clearly exhibits the inferiority of patterning at the outlet in terms of mixing enhancement. This trend can be explained by considering the recirculation zone reaches the outlet when the Al_2O_3 is patterned near the outlet. In order to maximize the mixing enhancement effect, the Al_2O_3 pattern must be attached at the inlet region so that the mixing effect due to the recirculation zone is completed before reaching a reaction zone of microreactors.

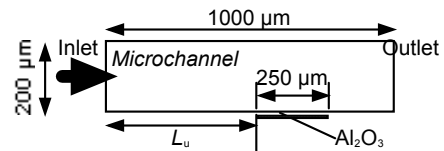


Fig.9 Configuration of the Al_2O_3 patterning for Fig. 10. Effect of the pattern position from the inlet, L_u , is discussed.

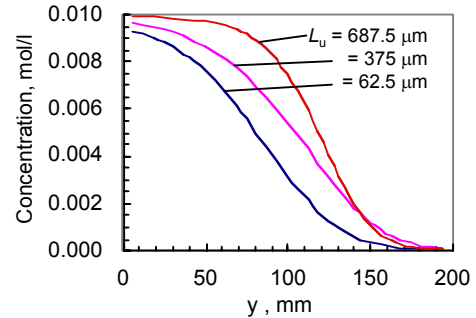


Fig.10 Calculated concentration profile at the channel outlet. The channel configuration is shown in Fig. 9.

The amount of lateral velocity component seems to be an important factor for mixing enhancement. More recirculation regions are intended by adding two Al_2O_3 patterns on the channel wall (Fig. 11), and the mixing enhancement is evaluated.

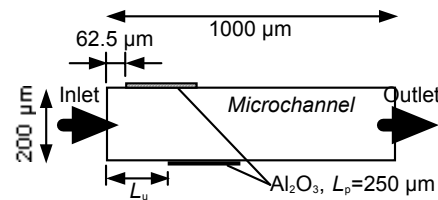


Fig.11 Configuration of the Al_2O_3 patterning for Fig. 12. Effect of the pattern position from the inlet, L_u , is discussed.

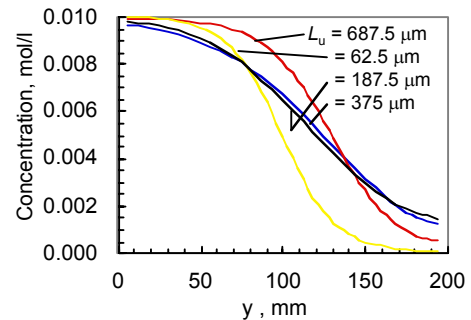


Fig.12 Calculated concentration profile at the channel outlet. The channel configuration is shown in Fig. 11.

The concentration profiles at the channel outlet (Fig. 12), exhibit the importance of the location of two Al_2O_3 patterns. When the two Al_2O_3 patterns are located at the same distance ($L_u = 62.5\ \mu\text{m}$), the mixing enhancement effect does not appear due to the compensation of the lateral velocity components created by the two Al_2O_3 patterns. By

changing the distance, L_u , the flow field is effectively changed to enhance the mixing.

The patterning material should also have strong impact on the mixing enhancement effect. Figure 13 and 14 compares the mixing enhancement effect of Al_2O_3 and TiO_2 of 250 μm length. The isoelectric potential value and the corresponding zeta potential at $\text{pH} = 6$ of TiO_2 are chosen to be 7 and 17.5 mV for the present calculation [16]. The figure clearly shows the superior performance of Al_2O_3 patterning due to the difference of EOF velocity to the value of SiO_2 channel wall.

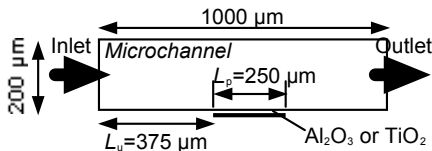


Fig. 13 Configuration of the Al_2O_3 patterning for Fig. 14. Effect of the patterned material is discussed.

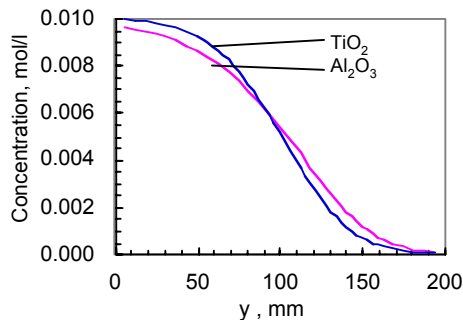


Fig. 14 Calculated concentration profile at the channel outlet. The channel configuration is shown in Fig. 13.

CONCLUSION

A novel microfluidic mixing device is proposed and examined in the present work. A sample device is fabricated to visualize the flow pattern change, and the results of numerical calculation suggest mixing enhancement effect. The device is expected to be used for various microsystems applications where mixing enhancement governs the system performance crucially.

ACKNOWLEDGMENT

Part of the sample fabrication has been conducted at the Mechanomicro Process Laboratory of Tokyo Institute of Technology, and the authors acknowledge the support of the faculties and staffs of the Lab. This work has been partly supported by the Kurata Memorial Hitachi Science and Technology Foundation and the Asahi Glass Foundation.

REFERENCES

- [1] Guenat, O.T., Ghiglione, D., Morf, W.E. and de Rooij, N.F., "Partial electroosmotic pumping in complex capillary systems, Part 2: Fabrication and application of a micro total analysis system (μTAS) suited for continuous volumetric nanotitrations", *Sensors and Actuators B*, Vol. 72, (2001), pp. 273-282.
- [2] Zhu, X and Kim, E.-S., "Acoustic-wave liquid mixer", *Microelectromechanical Systems (MEMS)*, ASME DSC-Vol.62/HTD-Vol.354, (1997), pp. 35-38.
- [3] Yi, M. and Bau, H.H., "The kinematics of bend-induced stirring in micro-conduits", *Micro-Electro-Mechanical Systems (MEMS)*, ASME MEMS-Vol.2, (2000), pp. 489-496.
- [4] L. Y.-K., Deval, J., Tabeling, P. and Ho, C.-M., "Chaotic mixing in electrokinetically and pressure driven micro flows", 14th IEEE Workshop on MEMS, (2001), pp. 483-486.
- [5] Yang, Z., Matsumoto, S., Goto, H., Matsumoto, M. and Maeda, R., "Ultrasonic micromixer for microfluidic systems", *Sensors and Actuators A*, Vol. 93, (2001), pp. 266-272.
- [6] Liu, R.H., Stremler, M.A., Sharp, K.V., Olsen, M.G., Santiago, J.G., Adrian R.J., Aref, H. and Beebe, D.J., "Passive mixing in a three-dimensional serpentine microchannel", *J. Microelectromechanical Systems*, Vol. 9, No. 2, (2000), pp. 190-197.
- [7] Nakata, M. and Fushinobu, K., Liquid mixing device, Japanese patent 2002-321508, (2002)
- [8] Nakata, M., Fushinobu, K. and Okazaki, K., "Micro fluid control device using surface properties", Proc. 6th ASME-JSME Thermal Engrg. Joint Conf., (2003), TED-AJ03-607.
- [9] Kosmulski, M., "Oxide/electrolyte interface: electric double layer in mixed solvent systems", *Colloids and Surfaces A*, Vol.95, (1995), pp.81-100
- [10] Kitahara, A., Furusawa, K., Ozaki, M. and Ohshima, H., "Zeta Potential", Tokyo, Scientist Co., Ltd., 1995
- [11] Kosmulski, M., "Attempt to Determine Pristine Points of Zero Charge of Nb_2O_5 , Ta_2O_5 , and HfO_2 ", *Langmuir*, Vol.13, (1997), pp.6315-6320
- [12] Parks, G.A., "The isoelectric points of solid oxides, solid hydroxides, and aqueous hydroxo complex systems", *Chemical Review*, Vol.65, (1965), pp.177-198
- [13] Rainey, P., Mitchell, S.J.N. and Gamble, H.S., "Flow Rate Measurement via Conductivity Monitoring in Microfluidic Devices", Proc. SPIE, Vol.4177, (2000), pp.185-193
- [14] Yang, R.-J., Fu, L.-M. and Lin, Y.-C., "Electroosmotic Flow in Microchannels", *J. Colloid and Interface Science*, Vol. 239, (2001), pp. 98-105.
- [15] Patankar, S.V., "Numerical Heat Transfer and Fluid Flow", Hemisphere, 1980.
- [16] Brookhaven Instruments Corp., homepage.